ANALYSIS OF THE PARAMETRIC-ACOUSTIC INSTABILITY FOR SAFETY ASSESSMENT OF HYDROGEN-AIR MIXTURES IN CLOSED VOLUMES

Yáñez, J., Kuznetsov, M., Redlinger, R., Kotchourko, A., Lelyakin, A.,

Institute for Energy and Nuclear Technique, Karlsruhe Institute of Technology, Kaiserstraße 12, 76131 Karlsruhe, Germany. Email jorge.yanez@kit.edu

ABSTRACT

The *acoustic* to the *parametric* instability has been studied for H_2-air mixtures at normal conditions. Two approaches for the investigation of the problem have been considered. The simplified analytical model proposed by Bychkov was selected initially. Its range of applicability resulted to be very restricted, and therefore, numerical solutions of the problem were taken into account. The results obtained were used to study the existence of spontaneous transition from the *acoustic* to the *parametric* instability for different fuel concentrations. Finally, the growth rate of the instabilities was numerically calculated for a set of typical mixtures for hydrogen safety

NOMENCLATURE LISTING

A	Auxiliary variable	Le	Lewis number	α	Auxiliary variable
a	Auxiliary variable	Ma	Markstein number	β	Auxiliary variable
B	Auxiliary variable	Pr	Prandtl number	γ	Auxiliary variable
C_1	Auxiliary variable	q	Auxiliary variable	δ	Auxiliary variable
C_2	Auxiliary variable	T_b	Temp. comb. products	ϑ	Dimensionless temp.
C_P	Heat at constant pressure	T_u	Temp. reactants	Θ	Expansion ratio
F	Flame front	U_a	Vel. of the acoustic field	κ	Auxiliary variable
g_a	Acceleration of gravity	U_L	Laminar flame velocity	λ	Thermal conductivity
H	Auxiliary variable	Y	Auxiliary variable	ρ	density
I	Auxiliary variable	z	Auxiliary variable	σ	Growth rate
J	Auxiliary variable	Ze	Zeldovich number	χ	thermal diffusivity
k	Wavenumber			ω	Frequency acoustic field
L	Laminar flame thickness			Ψ	Auxiliary variable

1 - INTRODUCTION

Generation of pressure waves by a flame in closed volumes is well known phenomenon. The interaction between those waves and the surface of the flame is a feed-back process in which pressure wave intensity and heat released by the flame influence each other. Markstein [1] concluded that the coupling between the both phenomena was due to the variation of the flame surface produced by the mechanism described here. The alternative velocity field created by the pressure waves produces oscillations of the amplitude of the cellular structures existing in the flames. This variation of the surface alters, in turn, the total amount of fuel consumed and the heat released by the flame.

Two different instabilities due to flame - pressure waves interaction have been identified [2]. In the *acoustic* instability (see [3]) the cellular structures of the flame front oscillate with the frequency of the acoustic alternative field. Two effects tend to muffle it. For large wavenumbers the instability is damped by diffusive processes. For small wavenumbers it is absorbed by the effect of gravity. The *acoustic* instability corresponds, for zero amplitude of the excitation velocity, to the *Darrieus-Landau* planar instability. For increased values of the alternative velocity [3], the *acoustic* instability has the notable property of being able to stabilize the *Darrieus-Landau* instabilty.

The *acoustic* instability is followed, for enhanced alternative velocity, by the *parametric* one. Under the later the growth rate is generally superior than in the *acoustic* case. The cellular structures of the flame oscillate with a frequency half of the *acoustic*, fact that was recognized by Markstein as the typical signal of the Kapitsa *parametrically* dumped pendulum, who consequently named so the instability.

From the point of view of the prediction of the severity of an explosion, the gaseous mixtures can be classified in two groups [5]. If the two instabilities co-exist for some ranges of acoustic velocities, a planar flame front is never stable and the *acoustic* instability transform spontaneously into the *parametric*. If they do not co-exist for any range of acoustic velocities, the *acoustic* instability tends to suppress the Darrieus-Landau instability, the *parametric* instability regime is never reached and planar flame fronts are stable as long as the alternative velocity field exists.

These two differentiate propagation regimes have been confirmed by the observations of Searby [8] and Aldredge and Killingsworth [7] who performed experiments with downwards propagating flames inside a cylindrical and an annular burner respectively. It was found that the flame propagation was divided in four differentiate stages. Just after ignition, the flame surface quickly became wrinkled due to the *Darrieus-Landau* instability and as the flame propagates further sound was generated. Due to the fundamental *acoustic* instability, these waves caused an attenuation of flame wrinkles. The *Darrieus-Landau* instability was suppressed and the flame became planar. Depending on whether the *parametric* and the *acoustic* instability coexist or not, the secondary *parametric* instability developed producing significant flame acceleration and the appearance of large organized pulsating cellular structures. In the final stage of development those coherent cellular structures were converted in incoherent flame surfaces fluctuations.

Therefore, gaseous mixtures prone to the *parametric* instability may suffer, in closed chambers, a very significant acceleration of the flame propagation velocity. Especially for lean mixtures, this increase of the combustion rate will be very considerable.

The mathematical treatment of the *acoustic* and *parametric* instabilities is based on the work of Pelce and Clavin [4], who obtained an equation for a perturbed flame front in a gravitational field. Based on those results, Searby and Rochwerger [5] managed to derive equations for the growth rate of the *acoustic* and *parametric* instability and were able to calculate the stability limits for both cases numerically. Some years later, Bychkov [6] simplified the previous formulation for the cases of small perturbation of a flame front and was able to obtain an analytical solution.

In the present study, the mentioned methodologies were applied to find out which mixtures tend to the *parametric* instability and which ones not under the typical conditions for hydrogen safety. The ranges of frequency and amplitude of the acoustic waves where the instability exists were identified for different hydrogen concentrations under normal pressure and temperature.

2 – ANALYSIS

The stability of a gaseous mixture with respect to the *acoustic* and the *parametric* instability can be calculated utilizing the methodology contained in the references [6], [5]. Let the flame front be represented by the function $F(\mathbf{x},t)=0$ in a reference commoving with the flame front. The small perturbations of the front could be considered in the form $F(x,t)=F(t)exp(ikx)$. Considering the problem linear, the second order differential equation (1) describes the evolution of small amplitude flame surface perturbations considering periodic velocity fluctuations normal to the flame front

$$A\frac{d^2F}{dt^2}+U_L\,k\,B\frac{dF}{dt}+k\,g_a\,C_1F-k\,\omega U_a cos(\omega t)\,C_1F+U_L^2\,k^2\,C_2F=0. \quad (1)$$

Where,

$$A=\left(1+\frac{\theta-1}{\theta+1}kL\left(Ma-\frac{\theta}{\theta-1}J\right)\right),\qquad B=\left(\frac{2\theta}{\theta+1}\left(1+\theta kL(Ma-J)\right)\right), \tag{2}$$

$$C_1=\left(\frac{\theta-1}{\theta+1}\left(1-kL\left(Ma-\frac{J\theta}{\theta-1}\right)\right)\right), \tag{3}$$

$$C_2=\left(\theta\frac{\theta-1}{\theta+1}\left(-1+\frac{kL}{\theta-1}\left((3\theta-1)Ma-2J\theta+2Prh_b(\theta-1)-I(2Pr-1)\right)\right)\right), \tag{4}$$

$$\vartheta=(T-T_u)/(T_b-T_u),\quad \gamma=(\rho_u-\rho_b)/\rho_u,\quad h(\vartheta)=\frac{\lambda(\vartheta)C_{P_u}}{\lambda_u C(\vartheta)}=\frac{\rho(\vartheta)\chi(\vartheta)}{\rho_u\chi_u}, \tag{5}$$

$$H=\int_0^1(h_b-h(\vartheta))\,d\vartheta,\quad J=\frac{\gamma}{1-\gamma}\int_0^1\frac{h(\vartheta)}{1+\vartheta\gamma/(1-\gamma)}d\vartheta,\quad I=(\theta-1)\int_0^1 h(\vartheta)\,d\vartheta, \tag{6}$$

$$Ma=\frac{J}{\gamma}-\frac{1}{2}Ze\left(Le-1\right)\int_0^1\frac{h(\vartheta)ln(\vartheta)}{1+\vartheta\gamma/(1-\gamma)}d\vartheta. \tag{7}$$

A very easy simplification may help to understand the meaning of the concept of *stability*. In the case $g_a=0$ and $U_a=0$, the temporal part of the solution of equation (1) has the form $F(t)=Y\exp(\sigma t)$ being Y a constant. Therefore, the planar flame front will be stable with respect to perturbations for all growth rates fulfilling $Re(\sigma)<0$ and unstable otherwise. In the more complex case under study, the solution is more complicated, see [12] (for Bychkov analysis $f(t)=f_1(t)+f_2\cos(\omega t)$) and [5] (see eq. (17)), but the concept remains.

2.1-Bychkov analysis

The analytical solutions obtained by Bychkov [12] were derived in the limit of high acoustic frequency and long wavelength flame surface perturbations. We will study whether the conditions to be fulfilled for their applicability are soundly satisfied.

2.1.1-Acosutic instability

In the case of the *acoustic* instability, for problems in which it is fulfilled that

$$\left|\frac{C_2U_L^2k^2}{A\omega^2}\right|\ll 1, \tag{8}$$

$$\left|\frac{C_1U_ak}{2A\omega}\right|\ll 1, \tag{9}$$

$$\left|\frac{C_1g_ak}{A\omega^2}\right|\ll 1, \tag{10}$$

the growth rate admits an explicit solution [6], and σ is directly,

$$\sigma = -\frac{B\,U_L\,k'}{2A} \pm \sqrt{\frac{(B\,U_L\,k)^2}{4A^2} - \frac{1}{A}\left(C_1 k\,g + C_2 U_L^2\,k^2 + \frac{C_1^2 U_a^2 k^2}{2A} \right)}. \quad (11)$$

Additionally, the border delimiting the instability region could be easily obtained,

$$\frac{U_a^2}{U_l^2} = -\frac{2Ag}{C_1 k' U_L^2} - \frac{2C_2}{C_1^2} A. \quad (12)$$

2.1.2-Parametic instability

Analogously, in the cases that

$$\left| \frac{C_1 U_a k}{A\omega} \right| \ll 1, \quad (13)$$

the growth rate for the *parametric* instability can be calculated solving the implicit equation

$$\left(A\sigma^2 - A\left(\frac{\omega}{2}\right)^2 + U_L kB\sigma + kgC_1 + U_L^2 kC_2 \right)^2 - \left(\frac{1}{2} k\omega U_a C_1 \right)^2 + \left(A\sigma\omega + \frac{1}{2} U_L kB\omega \right)^2 = 0. \quad (14)$$

And the line describing the border of the stable region is

$$2^2 k^2 \omega^2 C_1^2 U_L^2 \left(-A\frac{\omega^2}{2^2} + kgC_1 + U_L^2 kC_2 \right)^2 + \frac{B^2}{C_1^2} = \left(\frac{U_a}{U_L} \right)^2. \quad (15)$$

2.1.3- Particularization for H_2-Air mixtures in normal conditions

The equations appearing in previous sections were particularized for H_2-air mixtures at normal conditions. For every fuel concentration, the value of the molecular transport coefficient was obtained utilizing the molecular theory of gases [13]. The thermodynamic data was acquired using the JANAF tables [14]. The Lewis number of the mixture was calculated by means of the formulation proposed by Sun et al. [15]. Special care was taken to calculate the *overall* activation energy. The detailed chemistry scheme of Lutz [16] was coupled with the computer program Cantera [17] to obtain the *induction time* of the analyzed mixtures. This magnitude was then utilized to derivate the *overall* activation energy. The frequency of the acoustic perturbation ω, is a parameter which depends on the geometry of the particular problem to be addressed. The range of sizes of containers, tubes, deposits, etc. that practical safety assessments must cover is very wide. Typical examples would be from the analysis of combustion tubes (*~0.1* m of radius) to nuclear power plants (~ *25*. m radius). For the general purpose of our analysis, excitation frequencies from ω*=20* to *4000* Hz could be considered, which respectively correspond, for stoichiometric mixtures, to containers, buildings, etc. of 20, to 0.1 m of radius for the first harmonic.

The particularization of the equations (8-10) and (13) for the whole range of concentrations is represented in **Figure 1**. The curves relative to the equations (8-10) represent the maximum value for the left hand side (rhs) of those equations in the whole range of wavenumbers in which the instability takes place. The curve corresponding to the equation (13) describes the maximum values of its left hand side in the analyzed interval of wavenumbers (0-4000 m^{-1}). Out of the interval considered, the left hand side of the equation (13) is going to be even bigger, which substantiate the unusual shape of this curve. As can be seen in the figure, the values obtained for the left hand side of the equations (8) (9) and (13) for the H_2-air mixture under analysis are of the order of magnitude of 1. Therefore, the assumptions considered by Bychkov in his analysis are not fulfilled for our particular problem.

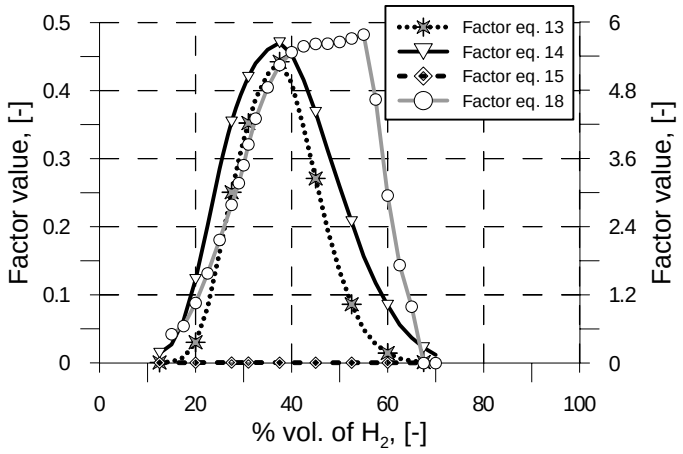

Figure 1. Values for the left hand sides of equations (8-10, 13). For the eq. (8-10) apply the left vertical axis; for eq. (13) right ordinates axis. The condition that those values are much smaller than one represents the necessary requirement for the validity of the Bychkov analysis assumptions. The curves were obtained for an excitation of ω=1000 Hz. Smaller frequencies will increase the values to be represented.

2.2-Numerical stability analysis

The equation (1) may be transformed for a more convenient treatment. The change of variables $\alpha = A,\ \beta = U_L kB,\ \psi = kg_a C_1 + U_L^2 k^2 C_2,\ \delta = k\omega U_a C_1$, allow writing the equation (1) as

$$\alpha \frac{d^2F}{dt^2} + \beta \frac{dF}{dt} + \left(\psi - \delta cos\left(\omega t\right)\right) = 0. \tag{16}$$

Which solution, as stated in [5], is of the kind

$$F = Y(z)e^{-\kappa z}e^{iky}, \tag{17}$$

where the new variables are defined as, $z = 12\omega t,\ \kappa = \beta\omega\alpha,\ a = 4\alpha\psi - \beta^2\omega^2\alpha$ and $q = 2\delta\omega^2\alpha$. The solution (17) is then substituted in (16). A much simpler differential equation for the variable Y appears,

$$Y'' + \left(a - 2q\right)cos\left(2z\right)Y = 0, \tag{18}$$

which is known as the Mathieu equation.

2.2.1-Mathieu equation

An extensive analysis of the solutions of the Mathieu equation may be found in [9]. Contrary to the procedure used by Searby and Rochwerger in [5], the Whittaker's method [10] was selected to obtain the solutions. It considers a solution for the Mathieu equation of the type,

$$Y(z) = e^{i\nu z}\sum_{k=-\infty}^{+\infty} c_{2k}e^{i2kz}. \tag{19}$$

Substituting this in (18), operating (details can be found in the references [12] and [11]) it is found that to be a solution, the variable ν should fulfill the condition

$$cos\left(\pi\nu\right)=1-\Delta(0,a,q)\left(1-cos\left(\pi\sqrt{a}\right)\right) \tag{20}$$

where

$$\Delta(\nu,a,q,k)=\begin{vmatrix} 1 & \gamma_{2k} & \cdots & & & & & & & & & & \\ \gamma_{2(k-1)} & 1 & \gamma_{2(k-1)} & \cdots & & & & & & & & & \\ \vdots & \vdots & \vdots & \ddots & \vdots & & & & & & & & \\ & & & \cdots & \gamma_2 & 1 & \gamma_2 & \cdots & & & & & \\ & & & & \cdots & \gamma_0 & 1 & \gamma_0 & \cdots & & & & \\ & & & & & \cdots & \gamma_2 & 1 & \gamma_2 & \cdots & & & \\ & & & & & & \vdots & \vdots & \vdots & \ddots & \vdots & \vdots & \vdots \\ & & & & & & & & & \cdots & \gamma_{2(k-1)} & 1 & \gamma_{2(k-1)} \\ & & & & & & & & & & \cdots & \gamma_{2k} & 1 \end{vmatrix} \tag{21}$$

with $\gamma_{2k}=q(2k-\nu)^2-a$. The Sträng method [11] allow calculating $\Delta(0,a,q,k)$ with the recursion formula,

$$\Delta(0,a,q,k)=\beta_{2k}\Delta(0,a,q,k-1)-\alpha_{2k}\beta_{2k}\Delta(0,a,q,k-2)+\alpha_{2k}\alpha_{2(k-1)}^2\Delta(0,a,q,k-3), \tag{22}$$

with $\alpha_{2k}=\gamma_{2k}\gamma_{2(k-1)}$ and $\beta_{2k}=1-\alpha_{2k}$ and $q,a\in\mathbb{R}$. This implies that $\gamma_{2i}\in\mathbb{R}\ \forall i\in\mathbb{N}$, so that $\Delta(\nu,a,q,k)\in\mathbb{R}$. Additionally, $a\in\mathbb{R}$ and so

$$cos(\pi\sqrt{a})=\begin{cases} cos(\pi\sqrt{a}) & a\geq 0 \\ cosh(\pi\sqrt{|a|}) & a<0 \end{cases}, \tag{23}$$

is always real. We may nevertheless study the solutions of $\nu\in\mathbb{C},\ \nu=u+wi,\ u,w\in\mathbb{R}$. Thus, $cos(i(u+wi))=cos(\pi u)cosh(\pi w)-isin(\pi u)sinh(\pi w)$ and them

$$cos(\pi u)cosh(\pi w)-isin(\pi u)sinh(\pi w)=1-\Delta(0,a,q)\left(1-cos\left(\pi\sqrt{a}\right)\right). \tag{24}$$

From the previous considerations,

$$cos(\pi u)cosh(\pi w)=1-\Delta(0,a,q)\left(1-cos\left(\pi\sqrt{a}\right)\right), \tag{25}$$

$$sin(\pi u)sinh(\pi w)=0. \tag{26}$$

The solutions of (26) are $u=0+k\pi$; or $w=0$. So, ν is purely real or complex. Therefore, the solutions of equation (25) are, if $w=0$

$$u=\frac{1}{\pi}acos\left(1-\Delta(0,a,q)\left(1-cos\left(\pi\sqrt{a}\right)\right)\right), \tag{27}$$

and if $u=0+k\pi$,

$$cosh(\pi w) = \pm\left(1-\Delta(0,a,q)\left(1-cos\left(\pi\sqrt{a}\right)\right)\right), \tag{28}$$

and so,

$$w = \pm\frac{1}{\pi}acosh\left(\left|1-\Delta(0,a,q)\left(1-cos\left(\pi\sqrt{a}\right)\right)\right|\right). \tag{29}$$

Thus, if $\left|1-\Delta(0,a,q)\left(1-cos\left(\pi\sqrt{a}\right)\right)\right| \le 1$, ν (see eq. (19)) is real, and otherwise complex. Recalling the definition of the solution,

$$Y(z) = e^{i(u+iw)z}\sum_{k=-\infty}^{+\infty} c_{2k}e^{i2kz} = e^{-wz}e^{iuz}\sum_{k=-\infty}^{+\infty} c_{2k}e^{i2kz}. \tag{30}$$

Substituting (19) in (17)

$$F = e^{-\kappa z}e^{iky}Y(z) = e^{-wz}e^{iuz}e^{-\kappa z}e^{iky}\sum_{k=-\infty}^{+\infty} c_{2k}e^{i2kz} = e^{(-w-\kappa)z}e^{i(uz+ky)}\sum_{k=-\infty}^{+\infty} c_{2k}e^{i2kz}, \tag{31}$$

that is stable in the case $-\nu < \kappa$. Due to the plus-minus solution of *w* eq. (29) it must happen that $|\nu| < \kappa$ and so,

$$\frac{1}{\pi}acosh\left(\left|1-\Delta(0,a,q)\left(1-cos\left(\pi\sqrt{a}\right)\right)\right|\right) < \frac{\beta}{\omega\alpha}. \tag{32}$$

And additional and very interesting conclusion is that, for the cases $\kappa < 0$, the stability is impossible.

2.2.2-Negative κ

The definition of κ was $\kappa = \frac{U_L kB}{\omega A}$. The variables U_L, k and ω are always positive. *A*, and *B* eq. (2) can be in principle positive or negative depending on the values of *Ma*, *J*, θ, *L*, and *k*. The Markstein number, because of the nature of the integrand can be written as

$$Ma = \frac{\theta}{\theta-1}J + \frac{1}{2}Ze\left(Le-1\right)\left|\int_0^1 \frac{h(\vartheta)ln(\vartheta)}{1+\vartheta(\theta-1)}d\vartheta\right|. \tag{33}$$

Applying (33)

$$A = \left(1+\frac{\theta-1}{\theta+1}kL\left(\frac{1}{2}Ze\left(Le-1\right)\left|\int_0^1 \frac{h(\vartheta)ln(\vartheta)}{1+\vartheta(\theta-1)}d\vartheta\right|\right)\right), \tag{34}$$

$$B = \frac{2\theta}{\theta+1}\left(1+\theta kL\left(\int_0^1 \frac{h(\vartheta)}{1+\vartheta(\theta-1)}d\vartheta + \frac{1}{2}Ze\left(Le-1\right)\left|\int_0^1 \frac{h(\vartheta)ln(\vartheta)}{1+\vartheta(\theta-1)}d\vartheta\right|\right)\right). \tag{35}$$

Defining k_{0A} and k_{0B} as the wavenumbers in which A and B change of sign (the condition $k_{0A} = 0$ represents a resonance)

$$k_{0A} = \frac{-1}{\frac{\theta-1}{\theta+1} L\left(\frac{1}{2} Ze\left(Le-1\right)\left|\int_0^1 \frac{h(\vartheta) ln(\vartheta)}{1+\vartheta(\theta-1)} d\vartheta\right|\right)}, \tag{36}$$

$$k_{0B} = \frac{-1}{\theta L\left(\int_0^1 \frac{h(\vartheta)}{1+\vartheta(\theta-1)} d\vartheta + \frac{1}{2} Ze\left(Le-1\right)\left|\int_0^1 \frac{h(\vartheta) ln(\vartheta)}{1+\vartheta(\theta-1)} d\vartheta\right|\right)}. \tag{37}$$

Remark that $Le-1$ is smaller than zero in case $Le<1$. For those cases, for $k > k_{0A}$ the coefficient A is negative, being

$$k_{0A} = -1\theta - 1\theta + 1L\left(\frac{1}{2} Ze\left(Le-1\right)\left|\int_0^1 \frac{h(\vartheta) ln(\vartheta)}{1+\vartheta(\theta-1)} d\vartheta\right|\right). \tag{49}$$

In the case that both $k_{0A}, k_{0B} \in \mathbb{R}^+$ there will exist a band of wavenumbers, if we suppose $k_{0A} < k_{0B}$ for wavenumbers k that are $0 < k_{0A} < k < k_{0B} < +\infty$, in which the flame is completely unstable. In the case only one of the values $k_{0A} \in \mathbb{R}^+$ or $k_{0B} \in \mathbb{R}^+$ then the band will extend to the infinite. Note additionally that this interval $0 < k_{0A} < k < k_{0B} < +\infty$ is independent of the value of the excitation frequency ω.

The solutions in which the variable κ is negative represent a significant instability mechanism. The gaseous mixtures in which $\kappa < 0$ result to be unstable for all intensities of the amplitude of the velocity perturbation for wavenumbers inside the range $[k_{0A}, k_{0B}]$. Due to this characteristic, in the opinion of the authors, this mechanism may be very prone to couple with the perturbations produced by waves, reflections, etc., in practical applications. Additionally, κ depend inversely on the frequency of the perturbation. Therefore, the greatest impact of the mentioned coupling mechanism would be for lean mixtures enclosed in big vessels.

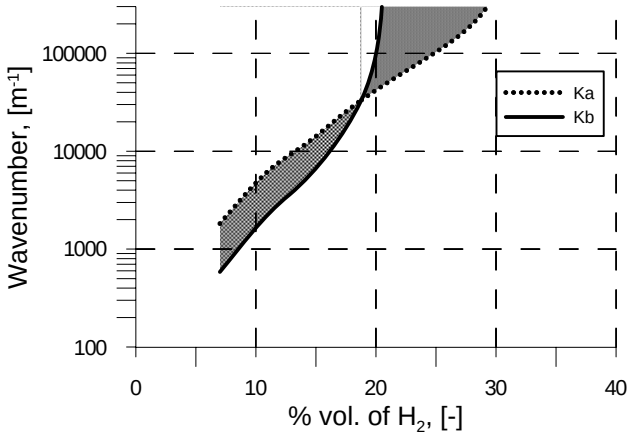

Figure 2. Bands of complete instability for different concentrations for hydrogen air mixtures in normal conditions.

2.2.3- Particularization for H_2-Air mixtures in normal conditions

The **Figure 2** contains the particularization of the variables k_{0A}, k_{0B} for H_2-air mixtures. It represent the limits in which the effect described in the previous section exists. For fuel concentrations superior to the 30% vol H_2, those mixtures are free from the existence of resonance. For lean mixtures, the band

on instability is centered in relatively low wavenumbers, fact that enhances the implication of the effect (see also **Figure 3** upper right).

The **Figure 3** contains the results of the application of the method for an excitation of 1000 Hz and normal conditions for fuel concentrations of 7.5, 12.5, 15., 30., 45., 60.% vol. H_2. The diagrams represent the growth rate in a colour scale for different combinations of flame surface wavenumbers (abscissa) and reduced velocities (ordinate). Only positive growth rates are plotted. The stable regions (pairs $(k, U_a/S_l)$ in which the growth rate σ is less or equal than 0) are plotted in violet. Black lines separate the stable regions from the unstable.

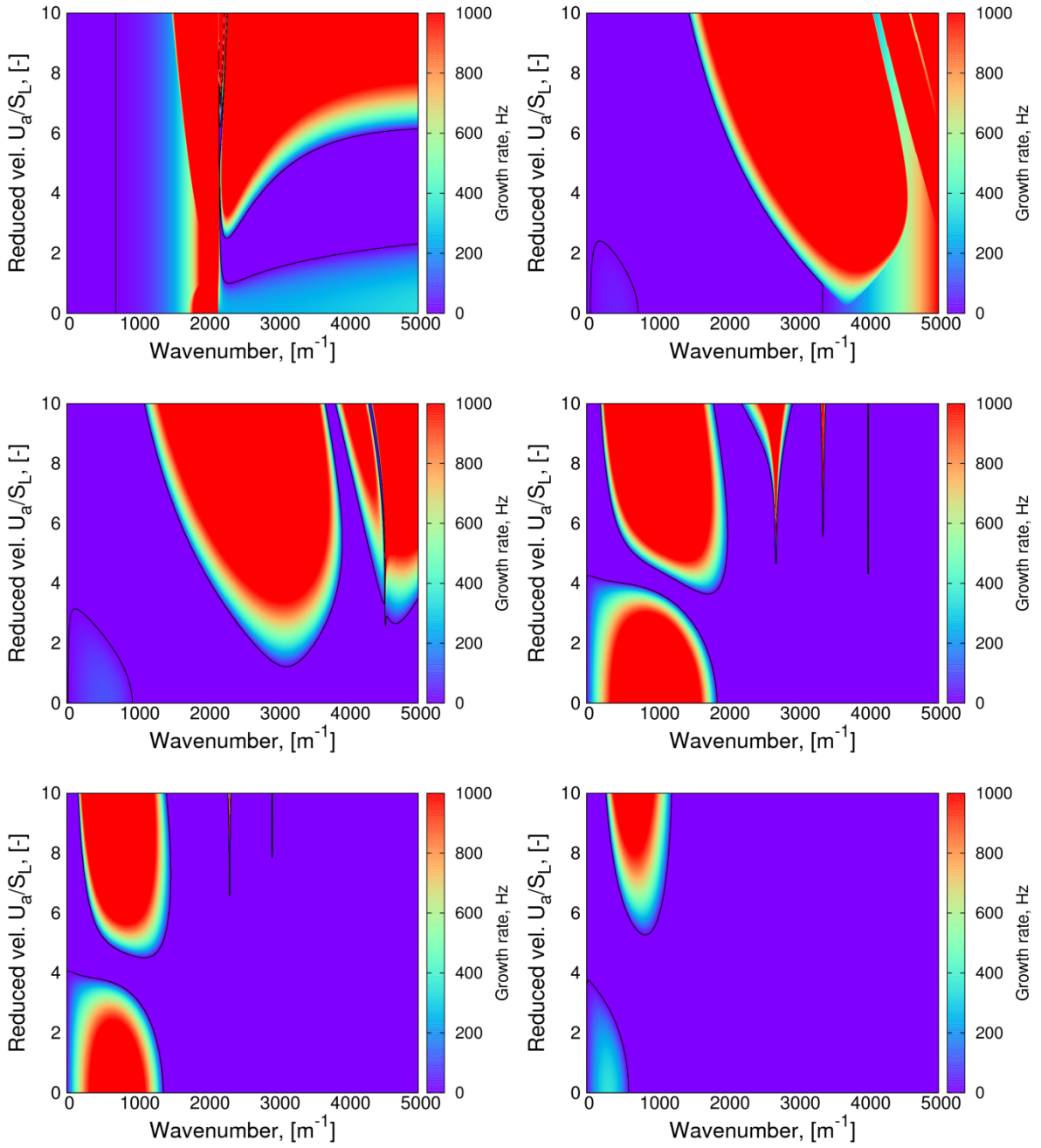

Figure 3. Stability graphs for H_2-air mixtures at normal conditions. Excitation frequency of 1000 Hz. From left to right and from top to bottom 7.5, 12.5, 15, 30, 45, 60 vol. H_2.

In the diagram corresponding to 7.5% it is represented the situation in which both $k_{0B}=0$ (left) and $k_{0A}=0$ (right, resonance) lines are visible (vertical lines). The stripe which lies between the lines is unstable. Left of this band appears a wavenumber range in which no positive growth rates are detected for the interval of reduced velocities considered. In the figure corresponding to 12.5 % H_2 only a small part of the $k_{0B}=0$ line is visible. The resonance lays in higher wavenumbers than the ones shown. Additionally, the *acoustic* instability (bottom left corner, still with a low growth rate) and the *parametric* instability (left) are clearly identifiable. The plots corresponding to 15% and 30% vol. H_2 show the appearance of the *acoustic* instability region with a growing intensity. Moreover, they depict a reduction of the overlap between the *acoustic* and the *parametric* instability. In the picture related to 45% vol. H_2, an horizontal stripe free of instability appears for intensities U_a/S_l of around 4.5. This band grows with an increased fuel concentration as it is shown in the plot for 60% vol. H_2. The absence of overlapping between both instabilities is a very interesting phenomenon. It not only prevents the spontaneous developing of the *acoustic* instability in the *parametric* but tends to the suppression of the DL instability (as higher U_a/S_l values produce negative growth rates)

Therefore, the thickness of the stripe free of any instability was investigated for perturbations of different frequencies and concentrations. The results obtained are plotted in the **Figure 4**. Some interesting conclusions can be obtained. Firstly, an enlarged perturbation frequency increases the thickness of the stability band. Also, higher perturbation frequencies enlarge the interval of concentrations in which the *acoustic* instability will not transform spontaneously into the *parametric*. In the extreme case of 20. Hz perturbations, no concentration interval resulted to be stable. This could be significant for the nuclear safety, in which the contention building, due to its size, will produce such order of magnitude of frequencies.

The frequency of the perturbation also changes the whole structure of the instability region. The **Figure 5** helps to understand the interesting and complex effect of the acoustic frequency. The stability diagrams for 20% vol. H_2-air mixtures at normal conditions are depicted for six different frequencies of 20., 100., 200., 600., 1000., 4000. Hz. The diagram corresponding to 20. Hz shows a complex overlapping between the *acoustic* and the *parametric* instability. Additionally, shows that the different *leafs* of the *parametric* instability come one after another without any stability *gap*. For higher frequencies, 100. Hz and more, there is a fine gap of stable region between the *parametric* and the *acoustic* instability meaning that two differentiate regions already exist. A further increase of the frequency will cause the displacement of the lobe corresponding to the *parametric* instability to higher wavenumbers. This displacement is very intense for the highest frequency considered of 4000. Hz (~ 10. cm wavelength for first harmonic in stoichiometric conditions).

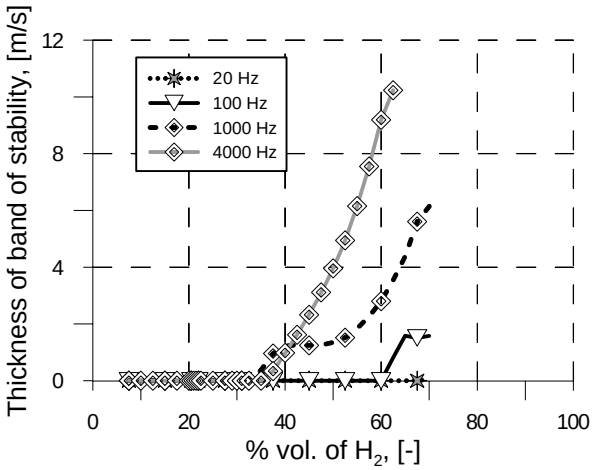

Figure 4. Amplitude of the stability band between the *acoustic* and the *parametric* instability.

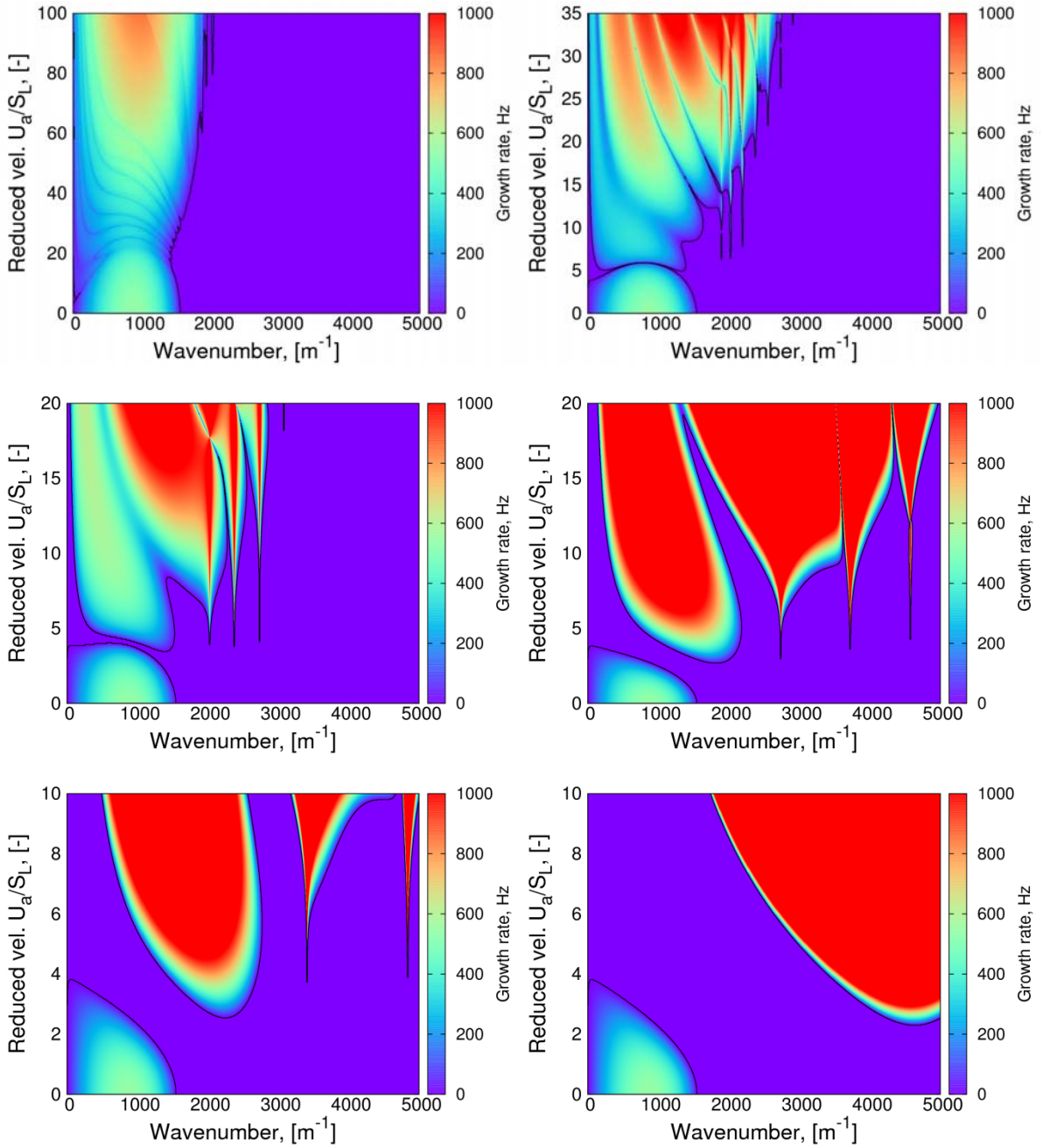

Figure 5. Stability graphs for 20% vol. H_2-air mixtures at normal conditions. From left to right and from top to bottom excitation frequency of 20, 100, 200, 600, 1000, 4000 Hz.

CONCLUSIONS

The analytical solutions obtained by Bychkov, due to the assumptions considered in its obtaining, resulted to be not applicable for H_2-air mixtures problems at normal conditions. The numerical analysis must then be used. The Mathieu differential equation, resulting from the derivation of this methodology, can be efficiently solved utilizing the Whittaker's method and the Sträng's formula. Utilizing this methodology, the stability of H_2-air mixtures at normal conditions was studied. It was shown that for concentrations leaner than 30% vol. H_2 the *acoustic* and the *parametric* instability always superposed. For richer mixtures, a stable *gap* between them that prevents a spontaneous transition from the former to the later appeared. The analysis was also performed for different excitation frequencies. It was found that, for small frequencies, the transition to *parametric* instability was unavoidable as the *parametric* and the *acoustic* instability superimposed in an intricate way. It

was ascertained that the thickness of the stability band increased with higher excitation frequencies. The results obtained show a very important dependency on concentration and excitation frequency that could be visualized in the diagrams plotted.

REFERENCES

1. Markstein, G. H., Non-steady flame propagation, 1964, Pergamon Press, New York
2. Searby, G., Acoustic instability in pre-mixed flames. Combustion Science and Technology. Vol. 81, No. 4–6, 1992, pp. 221–231
3. Pelce, P., Rochwerger, D., 1991 Vibratory instability of cellular flames propagating in tubes. J. Fluid Mech. 1999 Vol. 239, pp. 293–30.
4. Pelce, P, Clavin, P., Influence of hydrodynamic and diffusion upon the stability limits of laminar pre-mixed flames. J. Fluid Mech., 1982, Vol. 124, pp. 219-237.
5. Searby, G., Rochwerger, D., A parametric acoustic instability in pre-mixed flames. J. Fluid Mech., 1991, Vol. 231, pp. 529-543
6. Bychkov V., Analytical scalings for flame interaction with sound waves. Physics of Fluids, Vol. 11, Num. 10, 1999, pp. 3168-73.
7. Aldredge, R.C., Killingsworth N. J., Experimental evaluation of Markstein-number influence on thermoacoustic instability. Combustion and flame, Vol. 137, 2004, pp. 178-197
8. Searby, G., Acoustic instability in premixed flames. Combustion science and technology, Vol. 81, 1992, pp. 221-231.
9. Abramowitz, M., Stegun, I., Handbook of mathematical functions, 1972, Tenth Printing.
10. Whittaker, E.T., Watson, G. N., A course of modern analysis, fourth edition, 1962, Cambridge university press.
11. Sträng, J., E., On the characteristics exponents of Fouquet solutions to the Mathieu equation. ULM-TP/05-4
12. Jones, T., Mathieu's equation solution and stability. http://www.physics.drexel.edu/ im/open/mat/node3.html
13. Hirschfelder J.O., Curtiss C.F., Bird R.B., Molecular theory of gases and liquids, 1954, John Wiley and Sons, Inc., New York.
14. Malcolm W., Jr. Chase, Nist-Janaf Thermo-chemical Tables Set, 1998, Amer. Inst. of Physics Publ. Srvs.
15. Sun, C.J., Sung, C.J., He, L., Law, C.W., Dynamics of weakly stretched flames: quantitative description and extraction of global flame parameters. Combustion and flame vol. 118, 1999, pp. 108-128.
16. A.E. Lutz, Numerical Study of Thermal Ignition, Sandia Report SAND88-8228, 1988.
17. D.G. Goodwin, Cantera User's Guide, California Institute of Technology, Pasadena, CA, November, 2001